Long-term depression triggers the selective elimination of weakly integrated synapses

J. Simon Wiegert and Thomas G. Oertner[1]

Institute for Synaptic Physiology, Center for Molecular Neurobiology Hamburg, D-20251 Hamburg, Germany

Edited by Roger A. Nicoll, University of California, San Francisco, CA, and approved October 15, 2013 (received for review August 23, 2013)

Long-term depression (LTD) weakens synaptic transmission in an activity-dependent manner. It is not clear, however, whether individual synapses are able to maintain a depressed state indefinitely, as intracellular recordings rarely exceed 1 h. Here, we combine optogenetic stimulation of identified Schaffer collateral axons with two-photon imaging of postsynaptic calcium signals and follow the fate of individual synapses for 7 d after LTD induction. Optogenetic stimulation of CA3 pyramidal cells at 1 Hz led to strong and reliable depression of postsynaptic calcium transients in CA1. NMDA receptor activation was necessary for successful induction of LTD. We found that, in the days following LTD, many depressed synapses and their "neighbors" were eliminated from the hippocampal circuit. The average lifetime of synapses on nonstimulated dendritic branches of the same neurons remained unaffected. Persistence of individual depressed synapses was highly correlated with reliability of synaptic transmission, but not with spine size or the amplitude of spine calcium transients. Our data suggest that LTD initially leads to homogeneous depression of synaptic function, followed by selective removal of unreliable synapses and recovery of function in the persistent fraction.

long-term plasticity | transmitter release | dendritic spines | calcium imaging | channelrhodopsin

Long-lasting modifications of synaptic transmission are thought to underlie learning and information storage in the brain. Intact synaptic plasticity seems to be a precondition for memory formation, and disturbing long-term depression (LTD) or long-term potentiation (LTP) strongly interferes with learning (1–6). Hippocampal field potential recordings have been used to demonstrate that LTD and LTP can be stable for weeks in vivo, at least at the level of large synaptic populations (7–9). It is less clear, however, whether individual synapses can maintain their strength at a specific level over the time scales of memory. Commonly used recording techniques to assess synaptic plasticity (e.g., whole-cell recordings, field recordings, or imaging of Ca^{2+}-sensitive dyes) are too short-lived (10–12) or lack single-synapse resolution (7–9). Therefore, it is not known whether the strength of an individual synapse drifts over time, or how specific activity patterns affect the long-term stability of a synapse.

In vivo imaging experiments have shown that dendritic spines in mammalian cortex constantly change their morphology and sometimes completely disappear or form de novo (13–15). Life expectancy and turnover of spines is affected by experience and behavioral paradigms, suggesting a regulated, activity-dependent process controlling spine lifetime (16–19). Could LTP and LTD form the missing link between neuronal activity and lasting structural changes? Indeed, induction of LTP at individual excitatory synapses in vitro leads to increased spine head size (12) and insertion of postsynaptic scaffolding proteins (20) and glutamate receptors (21). Potentiation of individual spine synapses selectively increases their stability, pointing to a connection between synaptic plasticity and spine survival (22). Conversely, whether LTD is connected to spine shrinkage or a reduction in spine lifetime is less clear (23–27), as it was not possible to identify individual depressed synapses and to observe them over sufficiently long time periods. Because of these methodological limitations, we know little about LTD at the synaptic level: Are all synapses equally sensitive to depression-inducing activity patterns? For how long do individual synapses stay in the depressed state? Is LTD as synapse-specific as LTP, or does it spread to neighboring synapses?

To address these questions, we introduce a noninvasive, optical method based on optogenetic stimulation and two-photon Ca^{2+} imaging to control and measure the activity of individual hippocampal synapses in mature organotypic cultures over a period of 7 d. We found that depressed synapses were frequently eliminated from the circuit in the following days. This delayed elimination was not random: synapses with high release probability were more resistant to elimination than less reliable synapses. Resistant synapses were still connected to the same presynaptic axon after 1 wk and were indistinguishable from nonstimulated synapses, suggesting complete recovery of a subset of initially depressed synapses. Thus, the apparently stable LTD at the level of entire pathways in vivo does not seem to arise from a uniform, long-lasting depression of all stimulated synapses. On the contrary, it might reflect a protracted elimination process that removes a specific subpopulation of all depressed synapses. Our findings suggest that "long-term" depression of Schaffer collateral synapses following optogenetic low-frequency stimulation (oLFS) is, in fact, a transient phenomenon, setting in motion a reorganization of network connectivity.

Results

Optogenetic Stimulation and Optical Detection of Postsynaptic Calcium Transients. We used an adenoassociated viral vector to express an enhanced version of channelrhodopsin-2 [ChR2-E123T-T159C (28)] in a group of CA3 pyramidal cells (Fig. 1*A*).

Significance

Long-term plasticity, the ability of synapses to change their strength, is considered a possible basis of learning and memory. Extending the study of individual synapses to timescales relevant for behavior has been challenging: although rats can retain specific memories for several weeks, intracellular recordings that monitor the strength of individual synapses are typically limited to 1 h. Here we introduce an all-optical approach to stimulate and monitor synaptic function for 7 d. We show that long-term depression of hippocampal synapses significantly shortens their lifetime. While synapses with a high probability of transmitter release often recovered from depression, unreliable synapses were selectively removed from the circuit. Thus, specific activity patterns not only modulate synaptic weights but alter hippocampal connectivity.

Author contributions: J.S.W. and T.G.O. designed research; J.S.W. performed research; J.S.W. and T.G.O. analyzed data; and J.S.W. and T.G.O. wrote the paper.

The authors declare no conflict of interest.

This article is a PNAS Direct Submission.

[1]To whom correspondence should be addressed. E-mail: thomas.oertner@zmnh.uni-hamburg.de.

This article contains supporting information online at www.pnas.org/lookup/suppl/doi:10.1073/pnas.1315926110/-/DCSupplemental.

The construct included a red fluorescent label for synaptic vesicles (synaptophysin-tdimer2) to visualize light-activated presynaptic terminals (Fig. 1*B*). To detect excitatory postsynaptic Ca^{2+} transients (EPSCaTs) (10) in active spines, we coexpressed the genetically encoded Ca^{2+} indicator GCaMP3 (see *Materials and Methods*) and the bright CFP variant cerulean in two or more CA1 pyramidal cells by using single-cell electroporation (Fig. 1 *A* and *B* and Fig. S1*A*). The dynamic range of GCaMP3 was large and consistent in a sample of CA1 neurons ($\Delta F/F_0$: 1715 ± 71%, coefficient of variation, 0.12), with a signal-to-noise ratio (SNR) suitable for EPSCaT detection in spines (Fig S1 *B* and *C*). We used an optical fiber to locally illuminate CA3 with 2-ms light pulses and patch-clamped one transfected CA1 pyramidal cell to monitor light-induced EPSCs ("reporter neuron"; Fig. 1*C*). EPSCs in CA1 reporter neurons were delayed by 7 to 12 ms with respect to the blue light pulse, consistent with spike propagation along Schaffer collateral axons after optical spike initiation in CA3. Next, we identified active synapses on a second GCaMP3-expressing CA1 pyramidal cell. We scanned small regions along oblique dendrites, rapidly switching between focusing mode (cerulean, 810 nm excitation) and Ca^{2+} imaging (GCaMP3, 980 nm). We imaged each region five times, optically stimulating CA3 each time with two blue light pulses (2-ms pulses, interstimulus interval, 40 ms; Fig. 1*D*). By using this stimulation protocol in high Ca^{2+} artificial cerebrospinal fluid (ACSF; 4 mM Ca^{2+}), the probability of a bouton of an optically stimulated CA3 cell axon to release glutamate at least once was ~98% (*Materials and Methods*). Only few spines produced EPSCaTs (1–2% of total spines), consistent with the low density of labeled presynaptic terminals [0.06 ± 0.003 boutons per cubic micrometer, compared with an overall density of three boutons per cubic micrometer estimated from previous reports (29, 30)] and an average excitatory postsynaptic current (EPSC) of 1,813 ± 360 pA in the reporter neuron. Invariably, responsive spines were touched by boutons containing clusters of fluorescently labeled vesicles, indicating direct synaptic contact with a ChR2-expressing axon. When a responsive spine had been identified, line scans across the spine head and parent dendrite improved temporal resolution to 500 Hz (Fig. 1*E*). EPSCaTs were scored (Fig. 1*F*) when GCaMP3 responses exceeded 2σ of baseline noise (Fig. S2*A*). Failure trials were distributed symmetrically around zero, and no "EPSCaTs" were

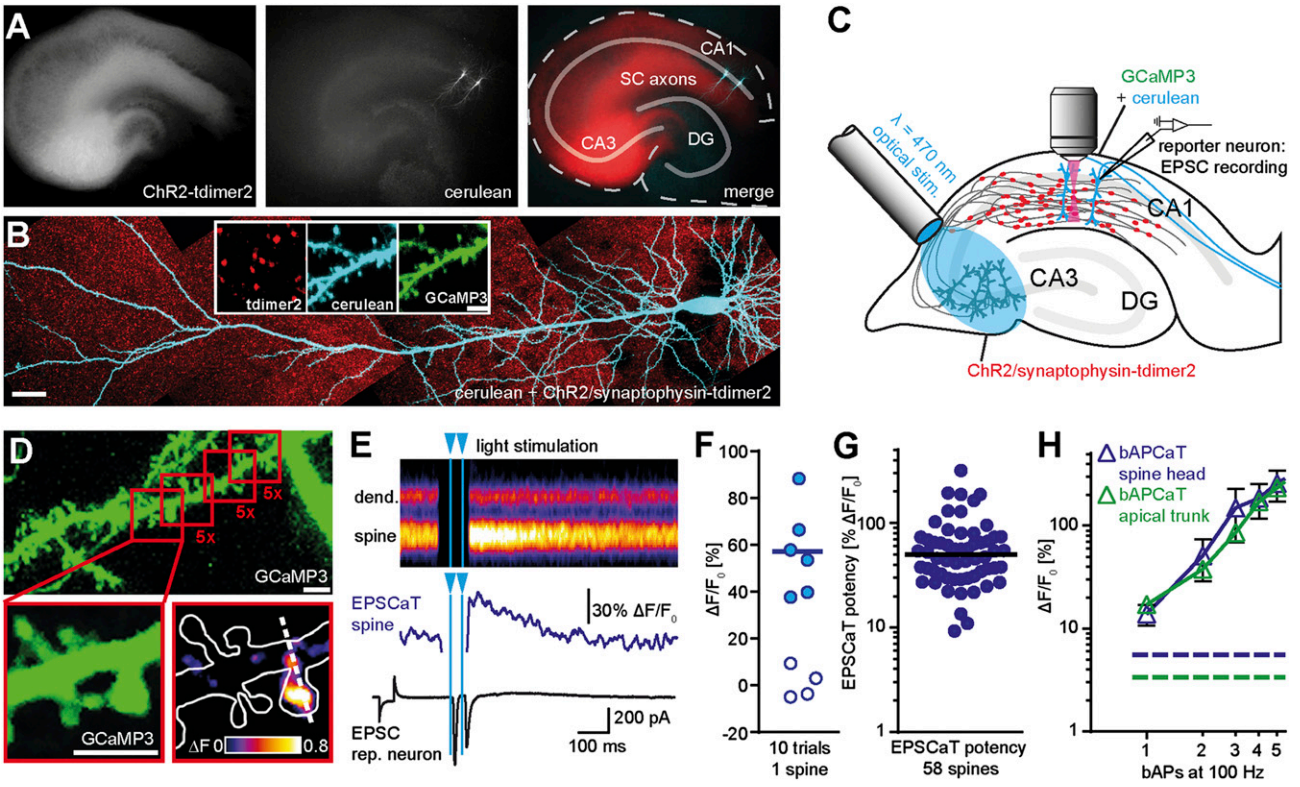

Fig. 1. Imaging optically induced spine calcium transients with GCaMP3. (*A*) Organotypic hippocampal slice at 23 days in vitro (DIV) expressing ChR2/tdimer2 in CA3 and GCaMP3/cerulean in two CA1 pyramidal neurons. (*Left*) Red fluorescence, freely diffusible tdimer2 labels ChR2/tdimer2-expressing CA3 neurons, and their axonal projections. (*Middle*) GCaMP3/cerulean transfected neurons in CA1. (*Right*) Merged image: solid lines mark cell body layers (DG, dentate gyrus; SC, Schaffer collaterals). (*B*) Two-photon maximum-intensity projection of GCaMP3/cerulean-expressing CA1 pyramidal cell. (Scale bar, 30 μm.) CA3 neurons express ChR2/synaptophysin-tdimer2 to visualize presynaptic vesicle clusters (red puncta). (*Inset*) Red fluorescence marks axonal boutons; GCaMP3 and cerulean are colocalized in dendrites and spines. (Scale bar, 3 μm.) (*C*) Experimental setup for optogenetic stimulation and spine Ca^{2+} imaging: A fiber-coupled LED (λ = 470 nm) was used to locally stimulate ChR2-expressing CA3 neurons. Spines on GCaMP3/cerulean-expressing CA1 pyramidal cells were imaged with two-photon microscopy. For parallel electrical recordings, a second GCaMP3/cerulean expressing neuron (reporter neuron) was patch-clamped. (*D*) Detection of active spines with GCaMP3 during presynaptic optogenetic stimulation. Stimulation-induced fluorescence changes (ΔF) of GCaMP3 were analyzed in fast frame scans (red squares) of oblique dendrites until a responsive spine was detected. Enlarged panels show an EPSCaT (F_0 and ΔF, single trial). (*E*) Line scans across spine head and parent dendrite (dashed white line in *D*) were used to quantify Ca^{2+} transients. The corresponding, temporally matched electrophysiological recording from the reporter neuron is plotted below the Ca^{2+} trace from the spine head. (*F*) Amplitude of 10 consecutive trials from a single spine. Open symbols indicate failure of synaptic transmission (Fig. S2). (*G*) Log-normal distribution of EPSCaT potency (median = 49.92% $\Delta F/F_0$, n = 58 spines). (*H*) Calibration of GCaMP3 using back-propagating APs (bAPCaTs; mean ± SEM). Dashed lines indicate detection threshold for Ca^{2+} transient detection (2σ of baseline) in dendrites (green) and in spines (blue).

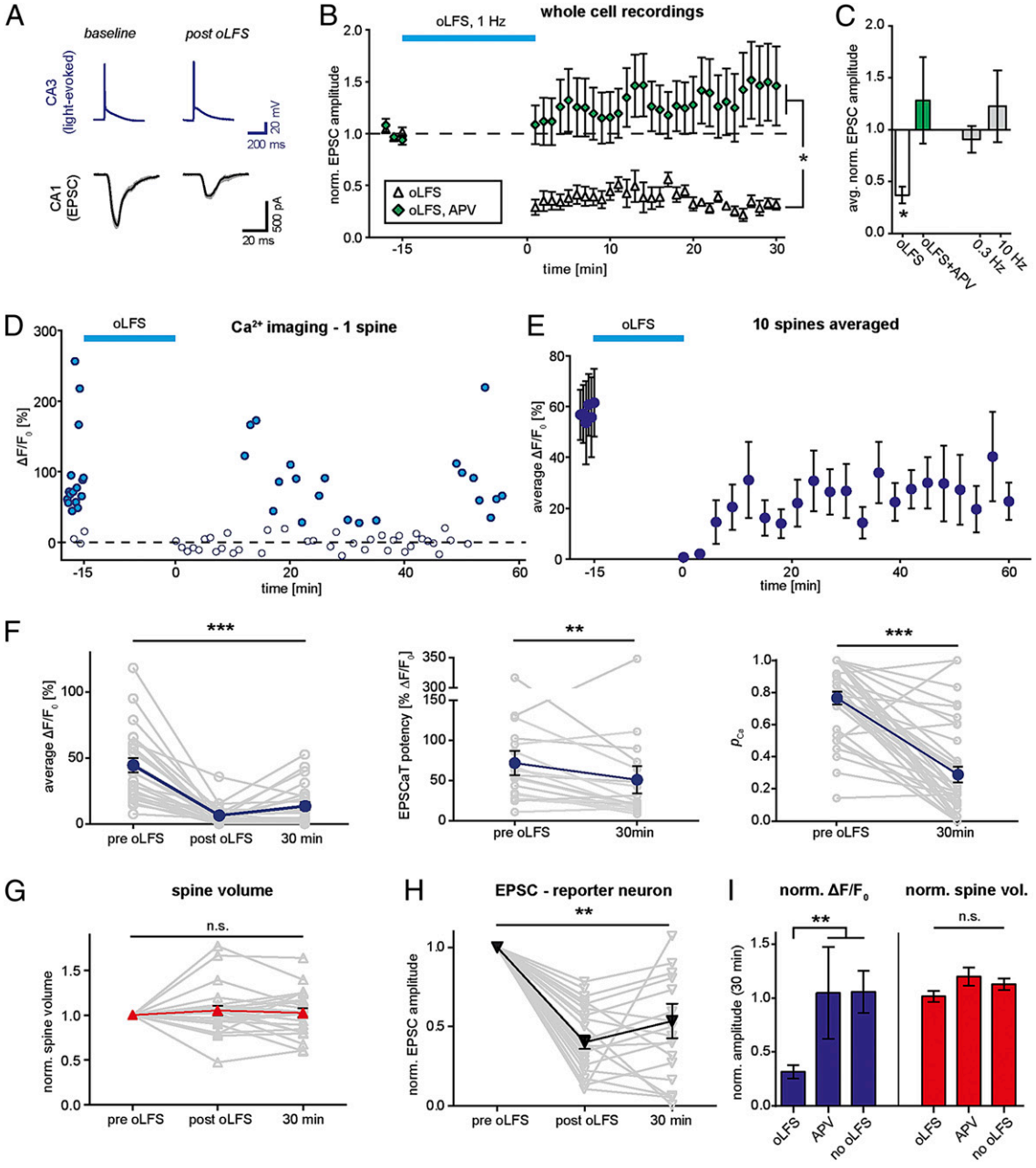

Fig. 2. Induction of LTD by optogenetic stimulation at 1 Hz. (*A*) Whole-cell recordings of LTD in CA1 and spiking reliability in CA3. Light pulses (2 ms, 0.1 Hz) were delivered to CA3 and light-evoked APs were recorded in a ChR2-expressing CA3 neuron. EPSCs were recorded in GCaMP3/cerulean-expressing CA1 pyramidal cells. oLFS (2-ms light pulses for 15 min at 1 Hz) induced LTD. Single-spike reliability in CA3 was 100%. (*B*) oLFS induced significant LTD (triangles; mean ± SEM; $n = 8$). Blocking NMDARs [50 μM D-2-amino-5-phosphonopentanoic acid (APV); green diamonds; $n = 8$] abolished LTD (*t* test). (*C*) Pharmacological profile and frequency dependence of optogenetic LTD induction (average of normalized EPSC amplitude 20 min after oLFS ± SEM vs. baseline; one-way ANOVA followed by Tukey test; $n = 8$ for 0.3-Hz and 10-Hz conditions). (*D*) EPSCaTs (filled blue markers) before and after oLFS in a stimulated spine. Frequency of paired test stimuli was reduced from 0.1 Hz before oLFS to 0.017 Hz after oLFS to minimize light exposure. Trials in which fluorescence transients did not exceed 2σ of baseline fluctuations were classified as failures (open blue markers). In this example, oLFS resulted in 50% depression of p_{Ca} and 11% depression of EPSCaT amplitude during the 60 min after oLFS. (*E*) Average Ca^{2+} transients were significantly depressed after oLFS (10 oLFS experiments; *t* test, $P = 0.002$). Each marker represents the average of three trials. (*F*) (*Left*) Average Ca^{2+} transients in directly stimulated spines before oLFS and immediately and 30 min after oLFS (gray) and mean of all spines [blue; $n = 28$ spines in 28 slice cultures; Friedman test (ANOVA) followed by Dunn test]. Separate analysis of EPSCaT potency (*Center*) and p_{Ca} (*Right*) in oLFS spines 30 min after oLFS: EPSCaT potency and p_{Ca} were significantly depressed (Wilcoxon signed-rank test). (*G*) Volume of stimulated spines (gray) and mean volume of all stimulated spines (red; $n = 26$; Friedman test). (*H*) Optically induced depression of EPSC amplitude in reporter neurons (gray) and mean of all neurons (black; $n = 26$; Friedman test followed by Dunn test). (*I*) Analysis of Ca^{2+} transients and spine volume 30 min after oLFS. Ca^{2+} transients were significantly depressed in oLFS spines compared with control conditions (blue bars; one-way ANOVA followed by Tukey test). When NMDARs were blocked during oLFS (APV; $n = 11$) or no oLFS was given ($n = 12$), Ca^{2+} transients were not depressed (*t* test against baseline). Spine volume was not different among the three groups (red bars; oLFS, $n = 26$; oLFS plus APV, $n = 11$; no oLFS, $n = 12$; one-way ANOVA followed by Tukey test). Error bars indicate ±SEM (*$P < 0.05$, **$P < 0.005$, and ***$P < 0.001$).

detected in dendrites (Fig. S2*B*). We define the average EPSCaT amplitude in a spine (excluding failures) as EPSCaT potency. The distribution of EPSCaT potencies was log-normal (Fig. 1*G*) as expected for random sampling of synapses. Median EPSCaT potency was comparable to the Ca^{2+} influx triggered by two to three back-propagating action potentials (APs; Fig. 1*H*), above the detection limit and well below saturation of GCaMP3 (Fig. S1).

Optogenetic Induction of LTD. Local blue light stimulation in CA3 reliably triggered single APs in CA3 cells that were followed by an EPSC in the postsynaptic CA1 cell. EPSC amplitude and spike threshold were nearly identical in GCaMP3-expressing and nontransfected neighboring CA1 cells (Fig. S3). oLFS (900 light-evoked APs at 1 Hz) induced pronounced LTD of optically induced EPSCs in GCaMP3-expressing neurons, but had no effect on the reliability of presynaptic spike generation (Fig. 2 *A* and *B*). As we had shown previously (31), GCaMP3 expression did not affect synaptic plasticity. Just like LTD induction by electrical LFS (32, 33), LTD induction by oLFS absolutely required NMDA receptor (NMDAR) activity (Fig. 2*B*). Moreover, LTD induction by oLFS was highly frequency-dependent and could not be induced at lower (0.3 Hz, 15 min) or higher frequencies (10 Hz, 900 APs; Fig. 2*C*). The pronounced frequency dependence excludes direct effects of blue light on synaptic function and is consistent with LTD induced by electrical LFS of Schaffer collaterals (32). In contrast to electrical stimulation, however, we could reactivate and test the same set of identified synapses on subsequent days.

Optical Detection of Depression at Individual Synapses. To investigate depression at individual synapses, we imaged postsynaptic Ca^{2+} transients using line scans across responsive spines and parent

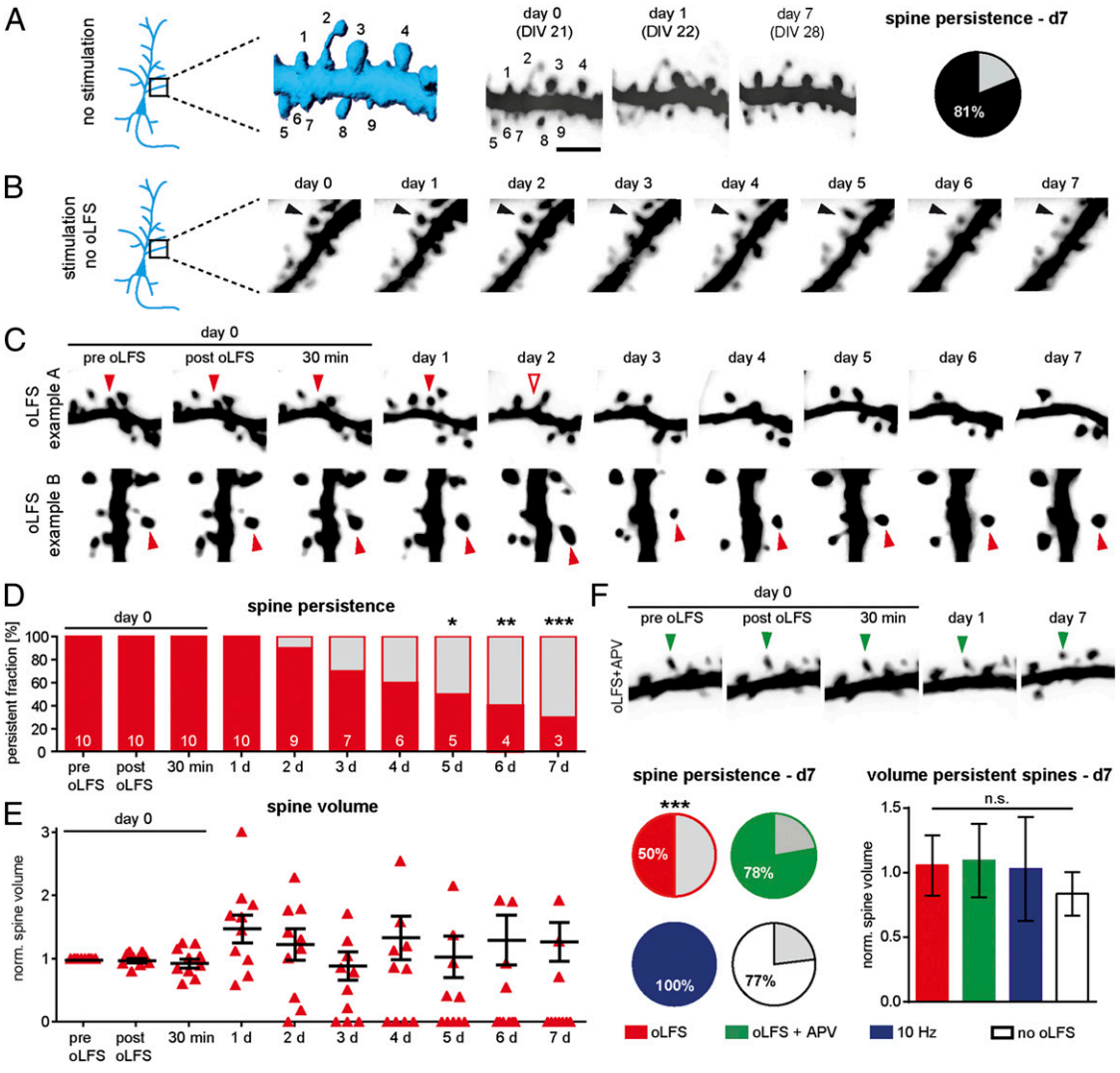

Fig. 3. LTD triggers delayed spine elimination. (*A*) Three-dimensional volume rendering and contrast-inverted maximum intensity projections of a segment from an oblique dendrite imaged at three time points without optical stimulation. Numbers indicate identical spines. (*Right*) Fraction of spines that persisted for 7 d (n = 135 spines in 12 slice cultures). (*B*) Dendritic segment harboring a responsive spine (arrowhead) imaged on seven consecutive days. (*C*) oLFS on day 0 triggered removal of spines in some (example A) but not all experiments (example B). Red arrowhead, oLFS spine; open arrowhead, time point of spine elimination. (*D*) Many depressed spines were eliminated during the days following oLFS (gray area, fraction of eliminated spines; solid red, fraction of persistent spines; numbers in white indicate persistent spines at each time point). (*E*) Mean volume of persistent oLFS spines (black lines) did not change over 7 d (n = 10 spines in 10 slice cultures, P = 0.481, Kruskal–Wallis test). (*F*) Analysis of spines imaged only at days 0, 1, and 7. (*Upper*) Blocking NMDARs during oLFS prevented spine loss (green arrowhead, oLFS spine). (*Lower*) Spine elimination was significantly enhanced only after oLFS (*Left*, gray areas). Volume of persistent spines (*Right*) had not changed 7 d after oLFS (red; n = 28), oLFS plus APV (green; n = 9), 10 Hz stimulation (blue; n = 4), or no oLFS stimulation (white; n = 13). Bars represent mean ± SEM (P = 0.996, one-way ANOVA). Error bars indicate ±SEM (*P < 0.05; **P < 0.005; ***P < 0.001.

dendrites (Fig. 1 *E* and *F*). After recording a series of Ca^{2+} transients as a baseline (paired-pulse stimulation at 0.1 Hz), we applied the oLFS protocol (900 single light pulses at 1 Hz) and continued to record Ca^{2+} transients for approximately 1 h (Fig. 2*D*). The use of paired pulses increases the probability of glutamate release and thus minimized the number of laser scans necessary to estimate synaptic strength. Immediately after oLFS, no EPSCaTs could be detected (Fig. 2*D*). Within the next 10 to 20 min, EPSCaT potency and EPSCaT probability (p_{Ca}) partially recovered, but remained depressed with respect to baseline. Averaging spine Ca^{2+} transients from 10 experiments revealed a strong and lasting depression as a consequence of oLFS (Fig. 2*E*), reminiscent of the depression of EPSC amplitude (Fig. 2*B*). To increase the size of our sample and further reduce light exposure of the synapses under scrutiny, we performed a larger set of oLFS experiments, imaging each spine in three time windows only: at baseline, immediately after oLFS, and 30 min after oLFS (10 trials each). Ca^{2+} transients were significantly depressed during 30 min after oLFS (Fig. 2*F*). Optical failure analysis 30 min after oLFS revealed depression of EPSCaT potency and p_{Ca} (Fig. 2*F*). In addition to the optical Ca^{2+} measurements, we monitored the volume of stimulated spines (*Materials and Methods*). Interestingly, whereas spine volume fluctuated in individual experiments, we did not observe systematic swelling or shrinkage of spines after oLFS (Fig. 2*G*). We conclude that, under conditions of sparse synaptic stimulation, strong functional depression can be induced without obvious effects on spine volume.

Recording electrical activity in a neighboring GCaMP3-expressing reporter neuron verified successful induction of LTD in each experiment (Fig. 2*H*). In agreement with electrically recorded LTD (Fig. 2*B*), no depression of spine Ca^{2+} transients was observed when APV was present during oLFS to block NMDAR function, or in experiments in which no oLFS was delivered (Fig. 2*I*). The volume of spines in these control experiments was not significantly different from oLFS spines after 30 min (Fig. 2*I*). After recording the acute effects of oLFS, cultures were transferred back into the incubator.

Delayed Elimination of Depressed Synapses. Before examining the long-term consequences of LTD, we characterized spine dynamics under control conditions for 7 d. Expression of GCaMP3 had no obvious effects on spine morphology or spine density (0.93 ± 0.07 spines per micrometer), which was similar to age-matched acute slices and slice cultures (34). The distribution of spine volumes (range, 0.002–0.446 μm^3; median, 0.0702 μm^3) matched data from perfusion-fixed CA1 pyramidal neurons (35). Over the course of 1 wk, spine density did not change significantly (net gain, 15 ± 11%) and 81% of all spines persisted (Fig. 3*A*). Head volumes of individual spines fluctuated strongly, but the average spine volume and the volume distribution remained constant (spine volume at day 0 vs. day 7; $P = 0.38$, Kruskal–Wallis test). Based on the characteristic branching pattern of the cell under scrutiny, the same dendritic segment could be reidentified at each imaging session, allowing us to track spines that were synaptically connected to light-stimulated axons (Fig. 3 *B* and *C*). Morphometric analysis was performed on 3D datasets (Fig. 3*A*); contrast-inverted maximum-intensity projections are shown for illustrative purposes.

To investigate the long-term consequences of LTD, we delivered oLFS to CA3 on day 0 and imaged synaptically connected spines in CA1 during the following 7 d (oLFS spines; Fig. 3*C*). To our surprise, many oLFS spines and their associated vesicle clusters disappeared during this week ($n = 7$ of 10; Fig. 3*D*). Volume changes in the persistent oLFS spines ($n = 3$ of 10) followed no particular direction, resulting in an average spine size similar to baseline conditions (Fig. 3*E*). To minimize light exposure of the cultures, we performed a second set of oLFS experiments (and controls) in which we collected data only at days 1 and 7 after plasticity induction (Fig. 3*F*). This larger dataset confirmed the delayed impact of oLFS on the persistence

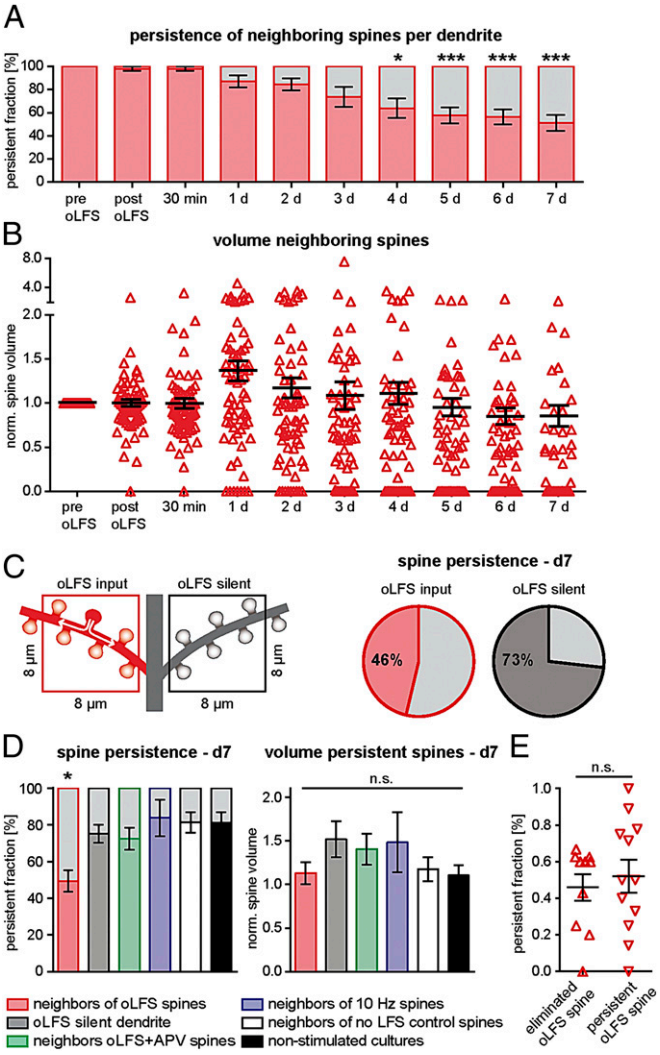

Fig. 4. Delayed elimination of nonstimulated neighbor spines. (*A*) Many nonstimulated spines next to oLFS spines (i.e., neighbors) were eliminated in the days following oLFS (red; mean persistent fraction of all neighbors on an 8–10-µm stretch of dendrite harboring an oLFS spine; $n = 10$ dendritic segments in 10 slice cultures; repeated-measures ANOVA). (*B*) The mean volume of persistent neighbors (black lines) did not change over 7 d ($n = 10$ slice cultures; $P = 0.174$, Kruskal–Wallis test). (*C*) Comparing oblique dendritic branches with (red square) or without an oLFS spine (black square) on the same neuron. Elimination of neighbors was more likely (54% lost, $n = 7$ dendrites in seven slice cultures) than elimination of spines on dendrites without oLFS spines (27% lost; $n = 7$). (*D*) Analysis of spines imaged at days 0, 1, and 7 under different conditions. (*Left*) Persistent (colored area) and eliminated fraction (gray area) of neighbors (red; $n = 28$ dendrites), spines on dendrites without oLFS spine (gray; $n = 7$ dendrites), neighbors in APV experiments (green; $n = 9$ dendrites), neighbors of spines receiving 10 Hz stimulation (blue; $n = 4$ dendrites), neighbors of responsive spines that did not receive oLFS (white; $n = 12$ dendrites), and spines in nonstimulated cultures (no Ca^{2+} imaging; black; $n = 12$ dendrites). Persistence was reduced in neighbors of oLFS spines only, not in any other group (mean ± SEM; one-way ANOVA followed by Tukey test, $^*P = 0.027$). (*Right*) Volume of persistent neighbors was not different from any of the control groups (mean ± SEM; $P = 0.06$, one-way ANOVA). (*E*) Fraction of neighbors persisting after oLFS until day 7 was not different between dendrites where the oLFS spine was eliminated (△; $n = 10$ dendrites; mean ± SEM) and dendrites where the oLFS spine persisted (▽; $n = 12$ dendrites; $P = 0.62$, unpaired t test). Error bars indicate ±SEM ($^*P < 0.05$ and $^{***}P < 0.001$).

of stimulated spines (50% lost vs. 19% lost in nonstimulated cultures at day 7; $P = 0.0002$) and their presynaptic terminals (Fig. S4). When NMDARs were blocked during oLFS or no oLFS was given, loss at day 7 was similar to nonstimulated cultures (APV, 22% lost, $P = 0.3$; no oLFS, 23% lost, $P = 0.24$). Stimulation with 900 pulses at 10 Hz did not induce loss of stimulated spines (0% loss; $P = 0.43$), consistent with the frequency dependence of LTD (Fig. 2*B*). In summary, reduced spine lifetime was only observed under conditions in which LTD was successfully induced.

The volume of the persistent oLFS spines after 7 d was unchanged compared with baseline (day 0) and not different from the three control groups (Fig. 3 *E* and *F*), suggesting that persistent oLFS spines had stabilized (normalized spine volume at day 7, oLFS spines, 1.06 ± 0.23; APV, 1.09 ± 0.28; 10 Hz, 1.03 ± 0.40; no oLFS, 0.84 ± 0.17). If spines persisted until day 7, were they still functionally connected to their associated presynaptic terminals, and, if so, did they recover from depression? We detected light-induced EPSCaTs in 81% ($n = 13$ of 16) of persistent oLFS spines and 80% ($n = 8$ of 10) of persistent control spines (no oLFS) at day 7. We noted, however, that dynamic range and sensitivity of GCaMP3 slowly decreased over time (Fig. S5). Therefore, instead of longitudinal analysis of Ca^{2+} transients, we decided to compare the amplitude between persistent oLFS spines and persistent control spines (no oLFS). The average Ca^{2+} amplitude in persistent oLFS spines, which was 27 ± 8% of that in control spines 30 min after oLFS, had significantly recovered ($P = 0.042$) at day 7 (to 75 ± 18% of the average Ca^{2+} amplitude in control spines). This indicates that the majority of persistent spine synapses had recovered from depression and was fully functional at day 7. In summary, depressed synapses were either entirely removed from the circuit or recovered from the depressive insult during the following days.

Delayed Elimination of Spines Neighboring Depressed Synapses. If extracellular electrodes are used to stimulate two separate sets of inputs, LTD is typically limited to the pathway receiving LFS [i.e., homosynaptic LTD (2)]. We were interested whether this pathway specificity is preserved at the micrometer scale. We evaluated changes in volume of all spines neighboring an oLFS spine on an 8-μm stretch of dendrite ("neighbors," Fig. 4*C*, red square). These neighbors did not display any detectable EPSCaTs upon light stimulation, indicating that no directly evoked synaptic input occurred during optogenetic LTD induction. Remarkably, we found that 54% of neighbors were also eliminated after oLFS (Fig. 4*A*). Similar to persistent oLFS spines, the average volume of persistent neighbors remained constant (Fig. 4*B*). Interestingly, elevated rates of spine removal were locally restricted to the neighborhood of oLFS spines (Fig. 3*C*). In the same neuron, spine elimination was not increased on dendritic branches that did not contain oLFS spines (elimination at day 7, oLFS dendrite, 50.7 ± 5.8%; oLFS-silent dendrite, 24.9 ± 4.9%; Fig. 4 *C* and *D*). Blocking NMDARs during oLFS, stimulating at 10 Hz, or omitting oLFS not only prevented removal of the stimulated spine (Fig. 3*F*), but also prevented increased elimination of neighbors (APV neighbors, 27.6 ± 5.9%; 10-Hz neighbors, 16.3 ± 9.9%; no-oLFS neighbors, 18.7 ± 5.5%; nonstimulated cultures, 18.8 ± 5.7; Figs. 3*B* and 4*D*), suggesting transfer of some signal to the neighbors is critical. In addition, we evaluated total spine density on day 7. In the vicinity of oLFS spines, but not on branches without oLFS spine on the same neuron, spine density was slightly reduced at day 7 (oLFS dendrite, 82 ± 7% of spine density at day 0, $P = 0.01$; no-input dendrite, 91 ± 9%, $P = 0.4$), indicating that the increased loss of spines around oLFS spines was partially compensated by an increased rate of spine formation. Remarkably, we found similar rates of spine elimination in the neighborhood of persistent and eliminated oLFS spines (Fig. 4*E*). This indicates that oLFS induced a comparable spread of depression in all experiments, irrespective of the fate of the directly stimulated spine, and raises the question why some spines were protected from elimination and others were not.

Calcium Transients, but Not Spine Volume, Correlate with Spine Survival After oLFS. Features predicting oLFS-induced elimination could be present at the synapse before oLFS (e.g., strength or reliability of the synapse) or may be revealed in a differential response to oLFS (e.g., changes in volume or Ca^{2+} signaling). To test predictability of spine elimination, we split our sample in two groups: Spines that were still present 7 d after receiving oLFS (persistent spines) and spines that did not survive after oLFS (eliminated spines). The immediate effects of oLFS were not different. Neither group showed an effect on spine volume, indicating that spines which were later eliminated did not shrink immediately after oLFS (Fig. 5*A*). Even on the day before elimination, spine volume was not reduced (before oLFS, 0.11 ± 0.03 μm^3; before elimination, 0.10 ± 0.03 μm^3), suggesting that oLFS-induced elimination occurred not as a gradual shrinkage over days, but was a relatively rapid process. The mean amplitude of Ca^{2+} transients was strongly depressed in both groups, both immediately (persistent spines, 87 ± 4% depression; eliminated spines, 88 ± 5% depression; $P = 0.76$) and 30 min after oLFS (persistent spines, 73 ± 9% depression; eliminated spines, 79 ± 10% depression; $P = 0.53$). Thus, the magnitude of functional synaptic depression did not determine the fate of the synapse days later.

Previous studies found a positive correlation between spine volume and synaptic strength (36–38). Larger spines, harboring stronger synapses, would be expected to be more resistant to oLFS-induced elimination (39). However, for directly stimulated spines and their neighbors, the initial volume of spines that were later eliminated was not different from the initial volume of persistent spines, and spine volume did not predict synaptic lifetime (Fig. 5*B* and Fig. S6). Interesting differences were revealed when we compared Ca^{2+} transients in the two groups before they were depressed by oLFS. Initial Ca^{2+} transients were significantly smaller in spines that were later eliminated (persistent spines, $\Delta F/F_0$, 55.3 ± 8.1%; eliminated spines, $\Delta F/F_0$, 24.0 ± 5.4%; $P < 0.01$; Fig. 5*C*). This was corroborated by a good correlation between spine lifetime and mean amplitude of the initial Ca^{2+} transients (Fig. 5*C*).

High p_{Ca} Protects Synapses from Elimination. As spines with larger mean Ca^{2+} transients were more likely to survive the days following oLFS, we sought to find out which synaptic parameters determined the differences in the Ca^{2+} signal. Larger average Ca^{2+} transients could result from a higher probability of glutamate release and thus more frequent EPSCaTs (p_{Ca}), or from larger postsynaptic Ca^{2+} currents, caused by a larger number of NMDARs or stronger postsynaptic depolarization, mediated mainly by AMPA receptors (40). To distinguish between presynaptic (p_{Ca}) and postsynaptic (EPSCaT potency) mechanisms, we performed EPSCaT failure analysis (Fig. S2) on all persistent and eliminated spines. We found no difference in initial EPSCaT potency of persistent and eliminated spines, and potency did not predict synaptic lifetime (Fig. 5*D*). However, the initial probability that paired-pulse light stimulation evoked an EPSCaT (p_{Ca}) was significantly higher in persistent spines (Fig. 5*E*). After paired-pulse stimulation, the probability of observing an EPSCaT is $p_{Ca} = 1 - (1 - p_{r1}) * (1 - p_{r2})$, with p_{r1} being the probability of synaptic glutamate release at the first pulse and p_{r2} the glutamate release probability at the second pulse. With 4 mM external Ca^{2+} and paired-pulse stimulation, p_{Ca} of persistent spines was 0.88 (median, before oLFS). Assuming no facilitation or depression, this corresponds to a single pulse $p_r = 1 - (1 - p_{Ca})^{1/2} = 0.65$. In eliminated spines, we found a p_{Ca} of 0.64, corresponding

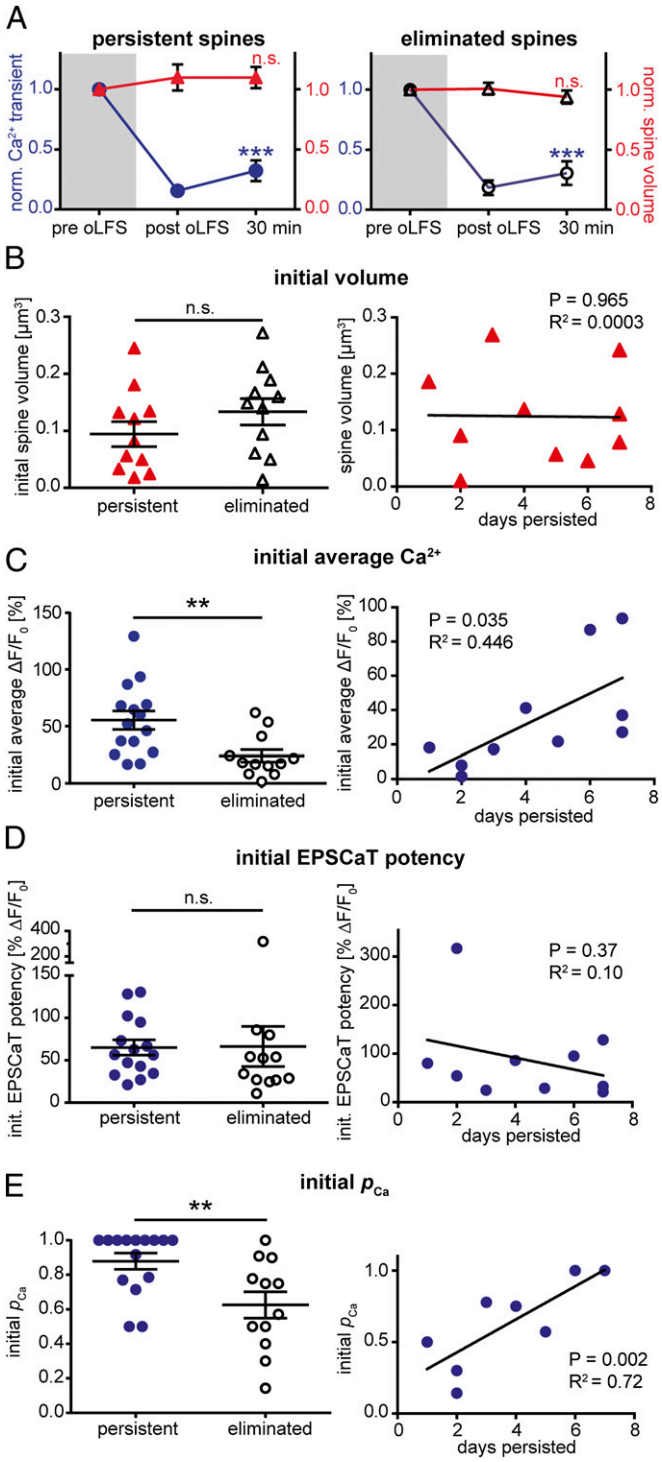

Fig. 5. Synapses with high p_{Ca} are resistant to oLFS-induced elimination. (*A*) Volume (red triangles; mean ± SEM; $P = 0.40$ for persistent spines, $n = 11$ spines in 11 slice cultures; $P = 0.37$ for eliminated spines, $n = 11$, repeated-measures ANOVA) and Ca^{2+} transients (blue circles; mean ± SEM; $P < 0.0001$ for persistent spines, $n = 15$; $P < 0.0001$ for eliminated spines, $n = 12$, Friedman test followed by Dunn test) were normalized to the value before oLFS and analyzed separately for spines that persisted until day 7 (*Left*) or were eliminated (*Right*). (*B*) (*Left*) initial volume of persistent spines (red triangles; $n = 11$) was not different from the initial volume of spines that were eliminated (open triangles; $n = 11$; $P = 0.232$, Mann–Whitney test). (*Right*) Regression analysis of spine persistence vs. initial volume shows no correlation ($n = 10$). (*C*) (*Left*) Initial mean Ca^{2+} transients were significantly larger in the group of spines that persisted until day 7 (persistent spines, blue circles, $n = 15$; eliminated spines, open circles, $n = 12$; $P = 0.0061$, Mann–Whitney test). (*Right*) Regression analysis of spine persistence vs. initial Ca^{2+} transients shows a positive correlation ($n = 10$). (*D*) (*Left*) Initial EPSCaT potency was not different in spines that persisted until day 7 (blue circles; $n = 15$ of 15) compared with spines that were eliminated (open circles, $n = 12$; $P = 0.986$, Mann–Whitney test). (*Right*) Regression analysis shows no correlation between initial EPSCaT potency and spine lifetime ($n = 10$). (*E*) (*Left*) Initial p_{Ca} was significantly larger in the group of persistent spines (blue circles; same spines as *D*; $P = 0.0092$, Mann–Whitney test). (*Right*) Regression analysis of spine persistence vs. initial p_{Ca} reveals a positive correlation (same spines as *D*). Black horizontal lines indicate mean ± SEM; n.s., not significant.

to a p_r of 0.40. Synapses with high initial p_{Ca} survived oLFS for a longer time (Fig. 5*E*). Importantly, EPSCaT potency was not correlated with p_{Ca} ($P = 0.17$, $R^2 = 0.073$), ruling out the possibility that EPSCaT detection was influenced by potency. As expected from random sampling, distribution of initial p_{Ca} and EPSCaT potency in the APV and no-oLFS control groups were similar to the oLFS group (oLFS, $p_{Ca} = 0.74 \pm 0.05$, EPSCaT potency = 65.74 ± 11.4; APV, $p_{Ca} = 0.76 \pm 0.08$, EPSCaT potency = 47.00 ± 5.74; no oLFS, $p_{Ca} = 0.64 \pm 0.08$, EPSCaT potency = 73.57 ± 19.65). Thus, enhanced spine loss after oLFS was not caused by some form of sampling bias (e.g., a lower initial p_{Ca} in this group compared with controls). We also investigated the spontaneous elimination of control spines, which was a rare event. Pooling data from no-oLFS and APV groups, we found no parameter that could predict spontaneous spine removal (Fig. S7). Thus, synapses with low p_{Ca} or low potency or small spine volume seem to be as stable as strong synapses under baseline conditions, but low p_{Ca} in combination with oLFS typically leads to elimination.

Discussion

Taken together, our data establish a causal link between LTD induction and the elimination of specific synaptic connections. We used oLFS of CA3 pyramidal cells to induce LTD at Schaffer collateral synapses in CA1. We show that optically induced LTD triggers destabilization of stimulated spines and their neighbors, often leading to their elimination days later. Not only were the postsynaptic elements removed, but presynaptic vesicle clusters also disappeared, indicating complete removal of the synapse (Fig. S4). Interestingly, the delayed elimination of depressed synapses was not a random process, but primarily affected synapses with an initially low probability of neurotransmitter release. The magnitude of depression was similar between persistent and eliminated synapses, suggesting that release probability had no direct effect on the efficacy of LTD induction (Fig. 5*A*). When no oLFS was applied, low release probability by itself had no measurable effect on spine lifetime (Fig. S7*B*). Thus, spine removal was indeed a consequence of LTD: spines that rarely receive synaptic input may be more susceptible to elimination if they are further weakened by LTD. As we show, LTD has a strong presynaptic component (Fig. 2*E*). This additional depression of glutamate release in the hours and days after oLFS might deprive LFS spines of an essential maintenance signal (41).

In previous studies, LFS was found to have a significant effect on spine turnover in young (26), but not in mature, cultures (23). Looking for several days, we now show extremely late effects of LTD induction in mature (3–4 wk in vitro) cultures that are well beyond the 3- to 5-h time window of these earlier studies. In addition, the ability to distinguish stimulated from nonstimulated spines enabled us here to quantify the effect of LTD on the lifetime of neighboring synapses, which was as strong as the effect on the stimulated synapse itself. As the LFS induction protocol takes several minutes, diffusible messengers such as activated protein phosphatases have ample time to travel from

the stimulated synapse to its neighbors, potentially mediating a local spread of depression (42, 43).

Spine removal looks gradual at the population level (Figs. 3 and 4), but seems to be a rather rapid process at individual synapses. At the last time point before disappearance, spine volume was not different from the average volume before stimulation. Thus, consistent with previous reports (23, 44), delayed spine removal is not the endpoint of a slow and gradual shrinkage process that starts immediately after LFS. Some studies (24, 27) reported immediate spine shrinkage after LFS, which we and others (23) did not observe. Glutamate photolysis at 0.1 Hz in Mg^{2+}-free solution (27) induces rapid shrinkage of a subset of spines. It is difficult to compare this protocol to the 1-Hz optogenetic stimulation we use here, as the activation profiles of ionotropic and metabotropic glutamate receptors and their downstream pathways were almost certainly different. Spine shrinkage was also observed upon electrical low-frequency activation of a local cluster of synapses, but not with a more distally placed stimulation electrode (24), corresponding to our distal optical stimulation in CA3. It seems that functional depression and spine shrinkage are mediated by separate molecular pathways that can be pharmacologically dissociated (25). Thus, spine shrinkage accompanies LTD in certain populations of spines (27) under specific stimulation conditions. Our oLFS protocol evoked transmission at a sparse and distributed set of synapses. It led to strong functional depression of activated synapses (Fig. 2), but apparently did not trigger rapid disassembly of the actin network in the stimulated spines.

As spine volume was not immediately reduced after oLFS, a different form of memory must exist to tag a locally confined set of synapses for later elimination. This tag could reside in the synapses themselves, or on the level of the dendrite. Depression of synaptic efficacy might have spread to neighboring synapses during oLFS (i.e., heterosynaptic depression). Spread of depression could be mediated by diffusion of LTD-specific signaling molecules (e.g., calcineurin and protein phosphatase 1) through the dendrite into neighboring spines (45). Alternatively, astrocytes could mediate heterosynaptic LTD (46). Subsequently, the weakened synapses might more likely be eliminated. On the contrary, depression could have induced lasting changes at the dendritic level that did not affect transmission at nonstimulated synapses. Potential mechanisms include branch-specific reduction in dendritic excitability (47), local changes in protein synthesis (48) or increased proteasomal degradation (49), or reduced transport to stimulated branches (50). These mechanisms are not mutually exclusive; several factors might contribute to synaptic destabilization after LTD.

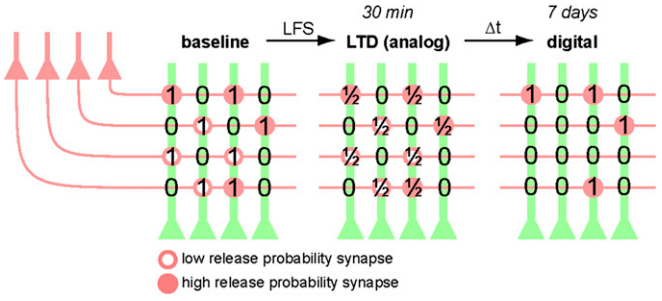

Fig. 6. Schematic illustration of analog-to-digital conversion. LFS of CA3 pyramidal cells (red) causes a reduction of synaptic weights (i.e., LTD) at all stimulated synapses. Within 1 wk (Δt), approximately half of the depressed synapses get eliminated, a process that alters the connectivity matrix between CA3 and CA1 (ones and zeros). High release probability synapses (filled circles) are more likely to survive and to recover from depression. In this cartoon, the number 1 was chosen to symbolize a hypothetical synaptic ground state and should not be taken as a claim that all Schaffer collateral synapses have identical strength. Synapse gain is omitted for clarity.

Based on field recordings of large synaptic populations in vivo (8), it has been assumed that the apparent long-term stability of LTP and LTD on the pathway level is reflected in stable adjustments of strength at the synaptic level. A comparable illusion of stable depression is produced in the present study when postsynaptic Ca^{2+} transients are averaged across many spines (Fig. 2*D*). Following the fate of individual synapses, however, suggests a different interpretation: The hippocampus seems to store information only transiently as analog adjustments of synaptic strength. Eventually, the stored information becomes encoded digitally as changes in the connectivity matrix between CA3 and CA1 pyramidal cells (Fig. 6). Theorists have long suggested that analog storage of information, via changes in strength of individual synapses, would be susceptible to degradation by synaptic drift and other forms of noise (51). Stable storage of information over long periods of time is most efficiently realized by binary encoding in a sparse matrix of connectivity (51, 52). The results of our long-time optical recordings suggest that analog and digital encoding strategies are used in the hippocampus for information storage, but on different time scales.

Materials and Methods

Slice Culture Preparation. Hippocampal slice cultures from Wistar rats were prepared at postnatal day 4 to 5 as described previously (53). No antibiotics were added to the culture medium. Animal procedures were in accordance with the guidelines of Directive 2010/63/EU and were approved by the veterinary office of Basel-Stadt, Switzerland.

Virus-Mediated Gene Expression. The cDNA sequences encoding ChR2-ET/TC-2A-tdimer2 or ChR2-ET/TC-2A-synaptophysin-tdimer2 were subcloned into a recombinant adenoassociated virus (rAAV)-vector under control of a human synapsin1 promoter. rAAV particles of the mosaic serotype 2/7 were obtained from the University of Pennsylvania (Gene Therapy Program Vector Core). For targeted viral transduction of CA3 at DIV 3, we pressure-injected (20 psi, 50 ms duration) 5 to 10 doses of virus under visual control (Dodt contrast) into CA3 stratum pyramidale using a Picospritzer III (Parker). Infected slices were kept in the incubator (5% partial pressure of CO_2) for an additional 2 wk to express the transgenes.

Single-Cell Electroporation. DNA encoding GCaMP3 (54) and cerulean were each subcloned into a neuron-specific expression vector (pCI) under the control of a human synapsin1 promoter. At DIV 18, single-cell electroporation was used to transfect CA1 pyramidal neurons in rAAV-infected slices with GCaMP3 and cerulean (ratio of 1:1). Plasmids were each diluted to 50 ng/μL in K-gluconate–based solution consisting of (in mM): 135 K-gluconate, 4 $MgCl_2$, 4 Na_2-ATP, 0.4 Na-GTP, 10 Na_2-phosphocreatine, 3 ascorbate, 0.02 Alexa Fluor 594, and 10 Hepes (pH 7.2). An Axoporator 800A (Molecular Devices) was used to deliver 50 hyperpolarizing pulses (−12 mV, 0.5 ms) at 50 Hz (55). Between DIV 21 and 28, expression of GCaMP3 and cerulean was largely stable (but see Fig. S5). GCaMP3 was excluded from the nucleus, and the ratio between GCaMP3 and cerulean fluorescence was constant in the transfected neurons, indicating intact Ca^{2+} handling. Morphology and spine density of neurons expressing GCaMP3 and cerulean was identical to neurons expressing cerulean alone.

Electrophysiological Characterization of Optogenetically Induced LTD. LTD experiments were performed between DIV 21 and 25. Whole-cell recordings from GCaMP3/cerulean-expressing CA1 pyramidal cells were made at 25 °C with a Multiclamp 700B amplifier (Molecular Devices) under the control of Ephus software written in Matlab (MathWorks) (56). Patch pipettes with a tip resistance of 3 to 4 MΩ were filled with (in mM): 135 K-gluconate, 4 $MgCl_2$, 4 Na_2-ATP, 0.4 Na-GTP, 10 Na_2-phosphocreatine, 3 ascorbate, and 10 Hepes (pH 7.2). To prevent burst firing, we recorded in high-divalent cation ACSF consisting of (in mM): 135 NaCl, 2.5 KCl, 4 $CaCl_2$, 4 $MgCl_2$, 10 Na-Hepes, 12.5 D-glucose, 1.25 NaH_2PO_4, 0.03 D-serine (pH 7.4, sterile filtered). Single APs were induced in ChR2(ET/TC)-expressing CA3 neurons with locally confined 2-ms pulses of blue light using a fiber-coupled LED (400-μm fiber, NA 0.37; Mightex Systems). Synaptic transmission before and after oLFS was measured in CA1 neurons in voltage clamp mode at a holding potential of −65 mV (junction potential corrected). During oLFS, CA1 neurons were held

in current-clamp mode. Access resistance was monitored continuously throughout the experiment, and recordings with a drift of more than 20% were discarded.

Two-Photon Microscopy. The custom-built two-photon imaging setup was based on an Olympus BX51WI microscope equipped with a LUMPlan W-IR2 60× 0.9 NA objective (Olympus), controlled by the open-source software package ScanImage (57). To activate ChR2(ET/TC)-expressing cells outside the field of view of the objective, we used a fiber-coupled LED to deliver light pulses directly to CA3 (as detailed earlier). A recording chamber with a 1-mm quartz glass bottom (WZW Optic) was used to minimize phosphorescence after the blue light pulse. Two ultrafast Ti:sapphire lasers (Chameleon Vision II; Coherent) controlled by electrooptic modulators (350-80; Conoptics) were used to excite cerulean (810 nm), GCaMP3 (980 nm), and synaptophysin-tdimer2 (980 nm), respectively. Emitted photons were collected through the objective and an oil-immersion condenser (1.4 NA; Olympus) with two pairs of photomultiplier tubes (PMTs; H7422P-40; Hamamatsu). Dichroic mirrors (560 nm) and emission filters (525/50, 607/70; Chroma Technology) were used to separate green and red fluorescence. Excitation light was blocked by short-pass filters (ET700SP-2P; Chroma Technology). During the blue light pulse, PMTs were protected by a shutter (NS45B; Uniblitz).

GCaMP3 Characterization. CA1 pyramidal neurons expressing cerulean and GCaMP3 were patch-clamped 3 to 5 d after electroporation (i.e., DIV 21–23), corresponding to the time when LTD experiments were started. Resting membrane potential of all recorded neurons was between −70 and −63 mV. To characterize the dynamic range of GCaMP3, 1, 2, 3, 4, 5, 10, 20, 40, 100, or 200 back-propagating APs were triggered at 100 Hz by somatic current injections (2–2.5 nA, 2 ms) in ACSF containing 50 μM APV and 10 μM 2,3-dihydroxy-6-nitro-7-sulfamoyl-benzo[f]quinoxaline-2,3-dione. Fluorescence was measured in line scan mode (500 Hz, 980 nm), and five trials were averaged per condition.

Measuring EPSCaTs. Frame scans (10 × 10 μm) of oblique dendrites were acquired to detect spines responding to optical stimulation of CA3 neurons. Two brief (2-ms) light pulses with an interpulse interval of 40 ms were applied to increase release probability and thus the chance of detecting responding spines. In each trial, 14 frames (64 × 64 pixel) were acquired at 7.8 Hz. To avoid false-negative spines caused by release failures, at least five trials were recorded from each dendritic segment. For an average synapse with a release probability, p_r, of 0.33 (58), the probability of synaptic failure (p_f) is $(1- p_{r1}) * (1 - p_{r2}) = 0.45$ during paired-pulse stimulation, assuming no facilitation or depression. In the five consecutive trials, p_f is $(0.45)^5 = 0.02$ or 2%. Thus, the probability of a stimulated synapse to release glutamate at least once is 98%. The relative change in GCaMP3 fluorescence ($\Delta F/F_0$) was calculated online. If the spine signal exceeded two times the SD of its resting fluorescence, this spine was considered as "potentially responding." To measure Ca^{2+} transients with better SNR, line scans were acquired across potentially responding spine heads and their parent dendrites (500 Hz, 10 trials per spine). Line scans were background-subtracted to remove any phosphorescence artifacts. To correct for bleaching, we fit an exponential decay to F_0 in a trial without light stimulation and subtracted the corresponding function from every stimulation trial. To measure the amplitude of Ca^{2+} transients and to distinguish successful synaptic transmission events (i.e., EPSCaTs) from failures, we used a template-based fitting algorithm. The characteristic decay time constant was extracted for every spine by fitting an exponential function to the average bleach-corrected GCaMP3 signal. To estimate the Ca^{2+} transient amplitude for every trial, we fit the spine-specific template to every response by using amplitude as the only free parameter. Response amplitude was defined as the value of the fit function at the time point at which the second light pulse occurred. A trace was classified as a "success" when its amplitude exceeded two times the SD (σ) of the baseline signal (Fig. S2).

Long-Term Imaging of Spine Morphology. The use of Hepes-buffered sterile-filtered ACSF allowed us to optically stimulate and image slice cultures under near-sterile conditions, using no perfusion system. The custom recording chamber (1 mm quartz glass bottom) and 60× water-immersion objective were sterilized with 70% (vol/vol) ethanol and filled with 1.5 mL sterile ACSF. A small patch of membrane (5 × 6 mm) supporting the hippocampal culture was cut out of the cell culture insert (PICM0RG50; Millipore), placed in the recording chamber, and weighted down with a U-shaped platinum wire with the use of gloves and sterilized tools (scalpel, forceps, pipettes). During imaging, the temperature of the slice culture was maintained at 25 °C via a permanently heated oil-immersion condenser (NA 1.4; Olympus). After each imaging session, the membrane patch was placed on a fresh sterile membrane insert and returned to the incubator. In the first imaging session, a spine displaying stimulation-induced EPSCaTs was centered, and a 3D image stack (*xy*, 10 × 10 μm; *z*, 5–15 μm) of the cerulean signal was acquired. Additional image stacks were acquired at low magnification to ensure identity of the dendritic segment. This procedure was repeated as indicated. For post hoc analysis of spine turnover, the 3D image stacks were aligned based on a rigid-body algorithm (ImageJ; National Institutes of Health). All spines identified in the 3D image stack acquired before oLFS were analyzed in the subsequent stacks, with the following exception: Spines that appeared shifted from their original position on the dendrite by more than 1 μm in any direction between two consecutive imaging sessions were not included in the analysis, as it was not clear whether the original spine was replaced by a new one. Filopodia were not included in the analysis. Maximum intensity projections are shown for illustrative purposes and were not used for analysis.

Spine Volume Measurements. The integrated fluorescence intensity of the spine head (cerulean) taken from a single optical section through the center of the spine was used to estimate its volume. For each cell, the maximum intensity was determined by immersing the point-spread-function (PSF) of the microscope in the apical trunk of the dendrite. In case of different depth of spine and calibration measurement, we corrected for laser attenuation in the tissue. The volume of the PSF was determined in image stacks of 100-nm fluorescent beads (Microspheres; Invitrogen). Knowing the volume of the PSF and the brightness of a given cell's cytoplasm allowed us to convert spine intensity into absolute spine volume (59).

ACKNOWLEDGMENTS. We thank Daniela Gerosa-Erni and Iris Ohmert for excellent technical support and Christine E. Gee and C. Peter Bengtson for critical comments on the manuscript. This study was supported by the Novartis Research Foundation and a Marie Curie Intra-European Fellowship within the Seventh European Community Framework Programme.

1. Martin SJ, Grimwood PD, Morris RG (2000) Synaptic plasticity and memory: An evaluation of the hypothesis. *Annu Rev Neurosci* 23:649–711.
2. Bear MF, Abraham WC (1996) Long-term depression in hippocampus. *Annu Rev Neurosci* 19:437–462.
3. Brigman JL, et al. (2010) Loss of GluN2B-containing NMDA receptors in CA1 hippocampus and cortex impairs long-term depression, reduces dendritic spine density, and disrupts learning. *J Neurosci* 30(13):4590–4600.
4. Lynch MA (2004) Long-term potentiation and memory. *Physiol Rev* 84(1):87–136.
5. Whitlock JR, Heynen AJ, Shuler MG, Bear MF (2006) Learning induces long-term potentiation in the hippocampus. *Science* 313(5790):1093–1097.
6. Moser EI, Krobert KA, Moser MB, Morris RG (1998) Impaired spatial learning after saturation of long-term potentiation. *Science* 281(5385):2038–2042.
7. Bliss TV, Gardner-Medwin AR (1973) Long-lasting potentiation of synaptic transmission in the dentate area of the unanaestetized rabbit following stimulation of the perforant path. *J Physiol* 232(2):357–374.
8. Abraham WC, Christie BR, Logan B, Lawlor P, Dragunow M (1994) Immediate early gene expression associated with the persistence of heterosynaptic long-term depression in the hippocampus. *Proc Natl Acad Sci USA* 91(21):10049–10053.
9. Staubli U, Lynch G (1987) Stable hippocampal long-term potentiation elicited by 'theta' pattern stimulation. *Brain Res* 435(1-2):227–234.
10. Enoki R, Hu YL, Hamilton D, Fine A (2009) Expression of long-term plasticity at individual synapses in hippocampus is graded, bidirectional, and mainly presynaptic: Optical quantal analysis. *Neuron* 62(2):242–253.
11. Harvey CD, Svoboda K (2007) Locally dynamic synaptic learning rules in pyramidal neuron dendrites. *Nature* 450(7173):1195–1200.
12. Matsuzaki M, Honkura N, Ellis-Davies GC, Kasai H (2004) Structural basis of long-term potentiation in single dendritic spines. *Nature* 429(6993):761–766.
13. Grutzendler J, Kasthuri N, Gan WB (2002) Long-term dendritic spine stability in the adult cortex. *Nature* 420(6917):812–816.
14. Trachtenberg JT, et al. (2002) Long-term in vivo imaging of experience-dependent synaptic plasticity in adult cortex. *Nature* 420(6917):788–794.
15. Holtmaat AJ, et al. (2005) Transient and persistent dendritic spines in the neocortex in vivo. *Neuron* 45(2):279–291.
16. Fu M, Yu X, Lu J, Zuo Y (2012) Repetitive motor learning induces coordinated formation of clustered dendritic spines in vivo. *Nature* 483(7387):92–95.
17. Hofer SB, Mrsic-Flogel TD, Bonhoeffer T, Hübener M (2009) Experience leaves a lasting structural trace in cortical circuits. *Nature* 457(7227):313–317.
18. Holtmaat A, Wilbrecht L, Knott GW, Welker E, Svoboda K (2006) Experience-dependent and cell-type-specific spine growth in the neocortex. *Nature* 441 (7096):979–983.

19. Lai CS, Franke TF, Gan WB (2012) Opposite effects of fear conditioning and extinction on dendritic spine remodelling. *Nature* 483(7387):87–91.
20. Ehrlich I, Malinow R (2004) Postsynaptic density 95 controls AMPA receptor incorporation during long-term potentiation and experience-driven synaptic plasticity. *J Neurosci* 24(4):916–927.
21. Hayashi Y, et al. (2000) Driving AMPA receptors into synapses by LTP and CaMKII: Requirement for GluR1 and PDZ domain interaction. *Science* 287(5461):2262–2267.
22. De Roo M, Klauser P, Muller D (2008) LTP promotes a selective long-term stabilization and clustering of dendritic spines. *PLoS Biol* 6(9):e219.
23. Nägerl UV, Eberhorn N, Cambridge SB, Bonhoeffer T (2004) Bidirectional activity-dependent morphological plasticity in hippocampal neurons. *Neuron* 44(5):759–767.
24. Zhou Q, Homma KJ, Poo MM (2004) Shrinkage of dendritic spines associated with long-term depression of hippocampal synapses. *Neuron* 44(5):749–757.
25. Wang XB, Yang Y, Zhou Q (2007) Independent expression of synaptic and morphological plasticity associated with long-term depression. *J Neurosci* 27(45): 12419–12429.
26. Bastrikova N, Gardner GA, Reece JM, Jeromin A, Dudek SM (2008) Synapse elimination accompanies functional plasticity in hippocampal neurons. *Proc Natl Acad Sci USA* 105(8):3123–3127.
27. Oh WC, Hill TC, Zito K (2013) Synapse-specific and size-dependent mechanisms of spine structural plasticity accompanying synaptic weakening. *Proc Natl Acad Sci USA* 110(4):E305–E312.
28. Berndt A, et al. (2011) High-efficiency channelrhodopsins for fast neuronal stimulation at low light levels. *Proc Natl Acad Sci USA* 108(18):7595–7600.
29. Mishchenko Y, et al. (2010) Ultrastructural analysis of hippocampal neuropil from the connectomics perspective. *Neuron* 67(6):1009–1020.
30. Shepherd GM, Harris KM (1998) Three-dimensional structure and composition of CA3—>CA1 axons in rat hippocampal slices: implications for presynaptic connectivity and compartmentalization. *J Neurosci* 18(20):8300–8310.
31. Huber D, et al. (2012) Multiple dynamic representations in the motor cortex during sensorimotor learning. *Nature* 484(7395):473–478.
32. Dudek SM, Bear MF (1992) Homosynaptic long-term depression in area CA1 of hippocampus and effects of N-methyl-D-aspartate receptor blockade. *Proc Natl Acad Sci USA* 89(10):4363–4367.
33. Mulkey RM, Malenka RC (1992) Mechanisms underlying induction of homosynaptic long-term depression in area CA1 of the hippocampus. *Neuron* 9(5):967–975.
34. De Simoni A, Griesinger CB, Edwards FA (2003) Development of rat CA1 neurones in acute versus organotypic slices: Role of experience in synaptic morphology and activity. *J Physiol* 550(pt 1):135–147.
35. Harris KM, Stevens JK (1989) Dendritic spines of CA 1 pyramidal cells in the rat hippocampus: serial electron microscopy with reference to their biophysical characteristics. *J Neurosci* 9(8):2982–2997.
36. Harris KM, Jensen FE, Tsao B (1992) Three-dimensional structure of dendritic spines and synapses in rat hippocampus (CA1) at postnatal day 15 and adult ages: implications for the maturation of synaptic physiology and long-term potentiation. *J Neurosci* 12(7):2685–2705.
37. Nusser Z, et al. (1998) Cell type and pathway dependence of synaptic AMPA receptor number and variability in the hippocampus. *Neuron* 21(3):545–559.
38. Matsuzaki M, et al. (2001) Dendritic spine geometry is critical for AMPA receptor expression in hippocampal CA1 pyramidal neurons. *Nat Neurosci* 4(11): 1086–1092.
39. Yasumatsu N, Matsuzaki M, Miyazaki T, Noguchi J, Kasai H (2008) Principles of long-term dynamics of dendritic spines. *J Neurosci* 28(50):13592–13608.
40. Holbro N, Grunditz A, Wiegert JS, Oertner TG (2010) AMPA receptors gate spine Ca(2+) transients and spike-timing-dependent potentiation. *Proc Natl Acad Sci USA* 107(36): 15975–15980.
41. McKinney RA, Capogna M, Dürr R, Gähwiler BH, Thompson SM (1999) Miniature synaptic events maintain dendritic spines via AMPA receptor activation. *Nat Neurosci* 2(1):44–49.
42. Yasuda R, Murakoshi H (2011) The mechanisms underlying the spatial spreading of signaling activity. *Curr Opin Neurobiol* 21(2):313–321.
43. Lisman J (1989) A mechanism for the Hebb and the anti-Hebb processes underlying learning and memory. *Proc Natl Acad Sci USA* 86(23):9574–9578.
44. Woods GF, Oh WC, Boudewyn LC, Mikula SK, Zito K (2011) Loss of PSD-95 enrichment is not a prerequisite for spine retraction. *J Neurosci* 31(34):12129–12138.
45. Collingridge GL, Peineau S, Howland JG, Wang YT (2010) Long-term depression in the CNS. *Nat Rev Neurosci* 11(7):459–473.
46. Chen J, et al. (2013) Heterosynaptic long-term depression mediated by ATP released from astrocytes. *Glia* 61(2):178–191.
47. Losonczy A, Makara JK, Magee JC (2008) Compartmentalized dendritic plasticity and input feature storage in neurons. *Nature* 452(7186):436–441.
48. Govindarajan A, Israely I, Huang SY, Tonegawa S (2011) The dendritic branch is the preferred integrative unit for protein synthesis-dependent LTP. *Neuron* 69(1): 132–146.
49. Bingol B, et al. (2010) Autophosphorylated CaMKIIalpha acts as a scaffold to recruit proteasomes to dendritic spines. *Cell* 140(4):567–578.
50. Janke C, Kneussel M (2010) Tubulin post-translational modifications: Encoding functions on the neuronal microtubule cytoskeleton. *Trends Neurosci* 33(8):362–372.
51. Chklovskii DB, Mel BW, Svoboda K (2004) Cortical rewiring and information storage. *Nature* 431(7010):782–788.
52. Poirazi P, Mel BW (2001) Impact of active dendrites and structural plasticity on the memory capacity of neural tissue. *Neuron* 29(3):779–796.
53. Stoppini L, Buchs PA, Muller D (1991) A simple method for organotypic cultures of nervous tissue. *J Neurosci Methods* 37(2):173–182.
54. Tian L, et al. (2009) Imaging neural activity in worms, flies and mice with improved GCaMP calcium indicators. *Nat Methods* 6(12):875–881.
55. Rathenberg J, Nevian T, Witzemann V (2003) High-efficiency transfection of individual neurons using modified electrophysiology techniques. *J Neurosci Methods* 126(1):91–98.
56. Suter BA, et al. (2010) Ephus: multipurpose data acquisition software for neuroscience experiments. *Front Neural Circuits* 4:100.
57. Pologruto TA, Sabatini BL, Svoboda K (2003) ScanImage: flexible software for operating laser scanning microscopes. *Biomed Eng Online* 2:13.
58. Oertner TG, Sabatini BL, Nimchinsky EA, Svoboda K (2002) Facilitation at single synapses probed with optical quantal analysis. *Nat Neurosci* 5(7):657–664.
59. Svoboda K, Tank DW, Denk W (1996) Direct measurement of coupling between dendritic spines and shafts. *Science* 272(5262):716–719.

Supporting Information

Wiegert and Oertner 10.1073/pnas.1315926110

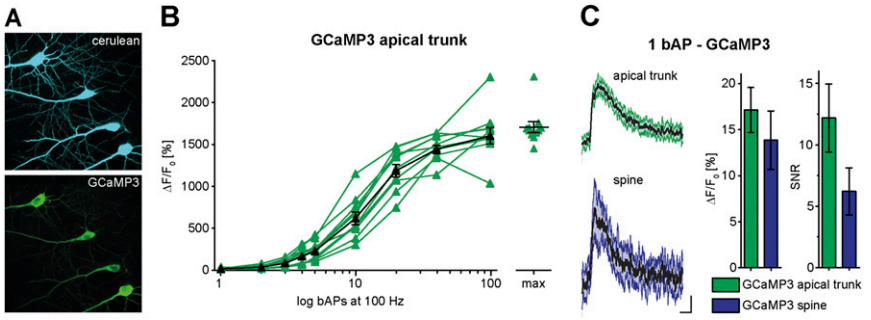

Fig. S1. Calibration of GCaMP3 performance using back-propagating action potentials (bAPs). (*A*) CA1 pyramidal cells expressing cerulean and GCaMP3 at 4 d after electroporation (21 days in vitro). (*B*) Calibrating GCaMP3 dynamic range with a series of bAPs at 100 Hz and two-photon line scanning at the proximal apical trunk. The dynamic range showed little variability between cultures as seen at the maximal response amplitude (n = 11 neurons from 11 slice cultures). (*C*) (*Left*) Mean traces of five GCaMP3 responses to one bAP measured in the proximal apical trunk (*Upper*; mean ± SD in green) and a spine head on a primary oblique dendrite (*Lower*; mean ± SD in blue). Calibration: 200 ms, 10% $\Delta F/F_0$. (*Right*) Mean Ca^{2+} transients and signal-to-noise ratios (SNRs) during one bAP measured with GCaMP3 in the proximal apical trunk (green) or a spine head on a primary oblique dendrite (blue; n = 10 neurons).

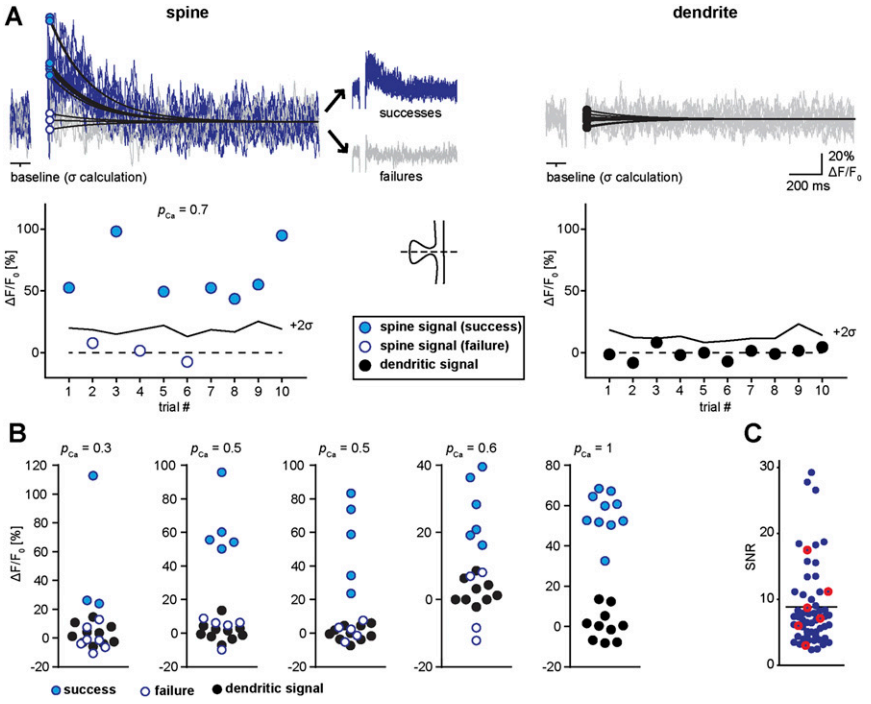

Fig. S2. Excitatory postsynaptic Ca^{2+} transient (EPSCaT) analysis. (*A*) GCaMP3 fluorescence transients were recorded simultaneously in the spine head (*Left*) and parent dendrite (*Right*). The amplitude of fluorescence transients was determined by fitting a template (single exponential function; *Materials and Methods*) to the fluorescence decay. Responses exceeding 2σ of baseline noise (calculated from the baseline signal of each trial) were classified as successes (blue traces and filled blue markers). Fluorescence fluctuations in the adjacent dendrite did not exceed 2σ of baseline noise (black markers). In each trial, CA3 pyramidal cells were stimulated by two light pulses at 40 ms interstimulus interval. (*B*) EPSCaT analysis in spines and their parent dendrites in five additional experiments, spanning low to high EPSCaT probability (p_{Ca}). Amplitudes and classification (filled/open markers) are shown for the first 10 trials. (*C*) SNR in spine Ca^{2+} measurements across all experiments (all stimulated spines). Markers with red outline indicate the six examples shown in *A* and *B*.

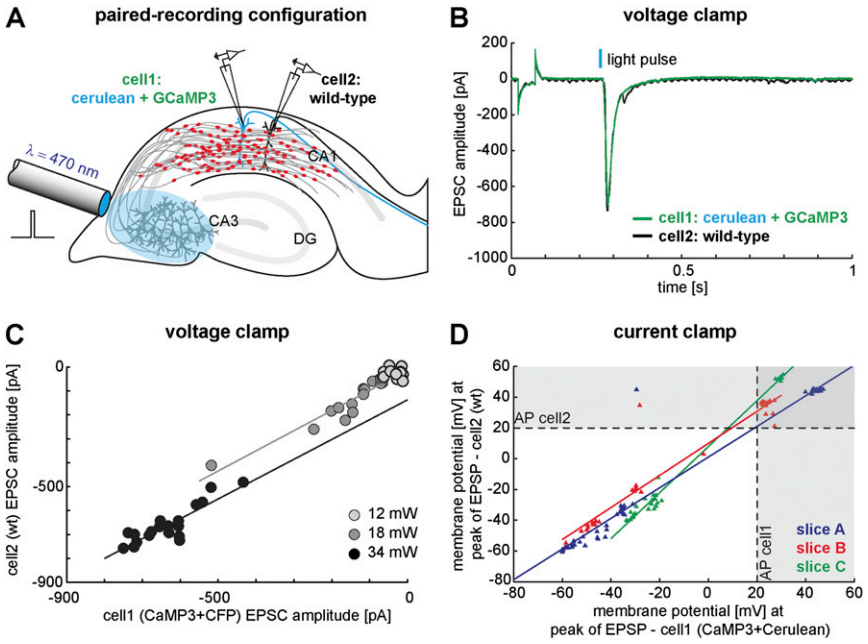

Fig. S3. Verification of "reporter neuron" strategy. (*A*) Schematic drawing of recording configuration. Paired recordings were made from two CA1 pyramidal neurons to compare light-evoked synaptic drive between the two. As only one of the two CA1 neurons was expressing GCaMP3/cerulean, these experiments were also used to rule out the possibility that overexpression of the two constructs affected synaptic transmission. (*B*) Representative light-evoked currents. For a given light pulse intensity, excitatory postsynaptic current (EPSC) amplitudes were similar in both neurons, indicating that a comparable number of synapses were activated. (*C*) Quantification of correlated synaptic input. EPSC amplitudes were highly correlated between pairs of CA1 neurons at different light intensities. EPSC amplitude in cell 2 is plotted against EPSC amplitude in cell 1 at three different light intensities. Each circle represents a single trial. Lines show linear regression function. (*D*) Postsynaptic membrane depolarization evoked by light-induced presynaptic APs is highly correlated between CA1 neurons. Peak membrane depolarization during the excitatory postsynaptic potential (EPSP)/AP of cell 2 vs. cell 1 is plotted for three independent experiments. In each experiment, the intensity of presynaptic light pulses was set to different values between 10 and 34 mW to recruit a variable number of CA3 cells. Colored triangles represent individual trials. Lines show linear regression function. Markers inside gray shaded area correspond to postsynaptic APs.

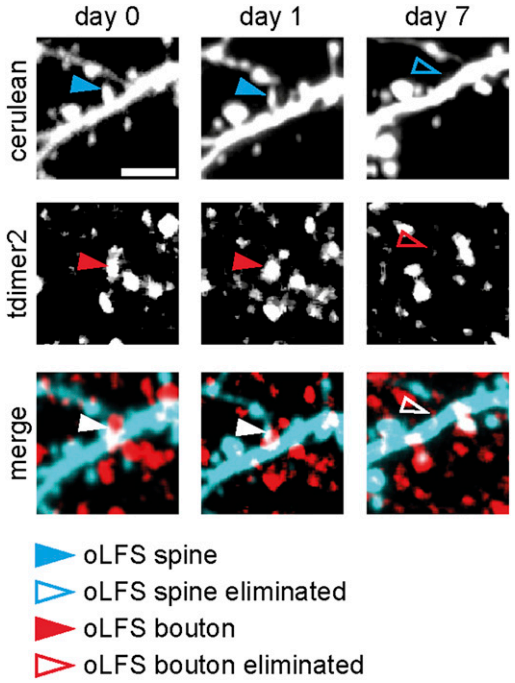

Fig. S4. Presynaptic vesicle cluster vanished with the elimination of optogenetic low-frequency stimulation (oLFS) spine. (*Top*) Maximum-intensity projection of cerulean signal before (day 0) and 1 and 7 d after oLFS. (Scale bar, 3 μm.) The oLFS spine is indicated by a cyan arrowhead. Open cyan arrowhead indicates dendritic location of eliminated spine at day 7. (*Middle*) Maximum-intensity projection of tdimer2 signal in the same volume. Red arrowhead indicates a bouton in contact with oLFS spine. Open red arrowhead indicates position of eliminated spine. Note absence of a red vesicle cluster at this position. (*Bottom*) Merged images.

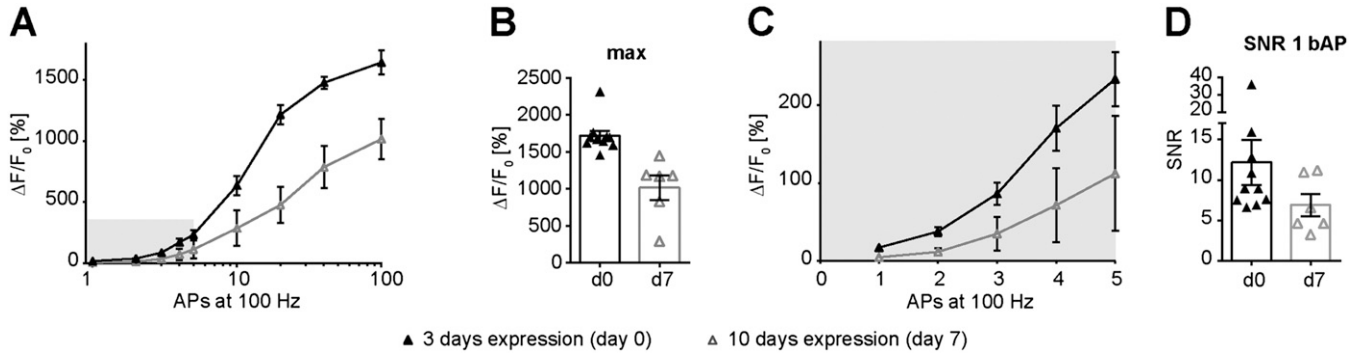

Fig. S5. Comparing GCaMP3 performance 3 d and 10 d after electroporation. (*A*) Average GCaMP3 responses in patch-clamped CA1 pyramidal cells using trains of bAPs (100 Hz) and two-photon line scanning at the proximal apical trunk. Black trace indicates neurons expressing GCaMP3 for 3 d [day 0 in long-term depression (LTD) experiment]. Gray trace indicates neurons expressing GCaMP3 for 10 d (day 7 in LTD experiment; $n = 6$ neurons in six slice cultures). (*B*) Maximum GCaMP3 response amplitude (200 bAPS at 200 Hz) is decreased at day 7 (10 d of expression) whereas variability is increased. (*C*) GCaMP3 responses to one to five bAPs are plotted on a linear *x* axis (shaded area from *A*). Note the smaller amplitude and the increased variability of GCaMP3 responses at day 7 (10 d of expression). (*D*) SNR for GCaMP3 responses evoked by one bAP is decreased at day 7 (10 d of expression).

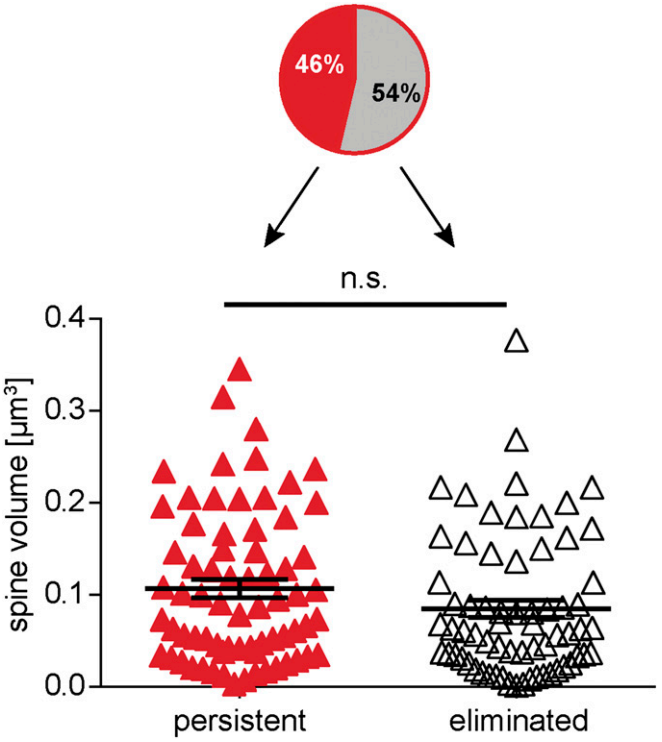

Fig. S6. Volume of neighboring spines does not predict persistence. The initial volume of spines next to oLFS spines that persisted for 7 d (red triangles; $n = 67$ spines) was not different from the initial volume of spines next to oLFS spines that were eliminated (open triangles; $n = 70$ spines). Black lines indicate mean ± SEM; $P = 0.09$, Mann–Whitney test, two-sided.

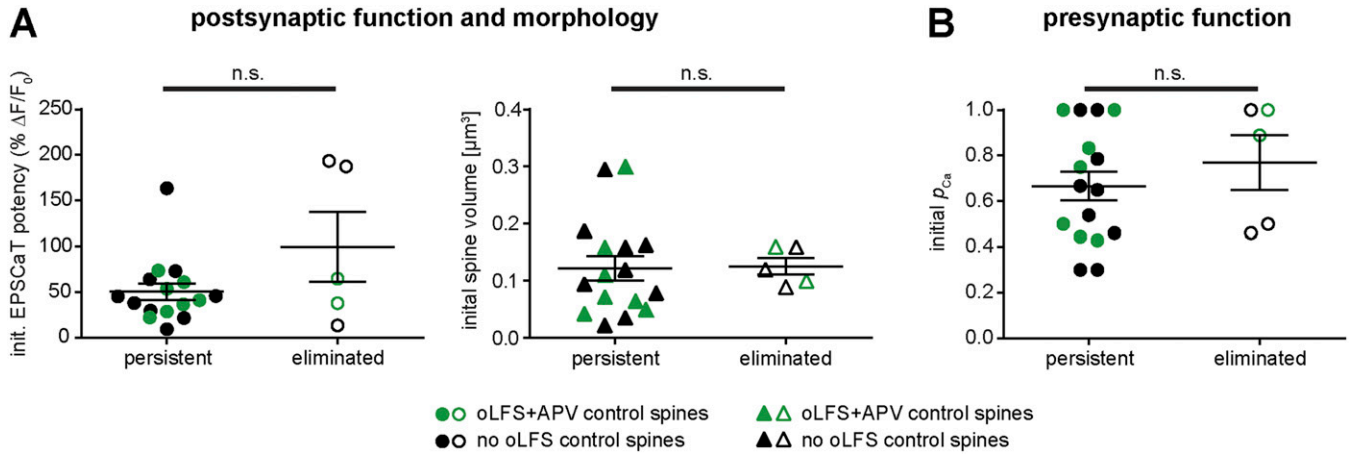

Fig. S7. Initial properties of persistent vs. eliminated control spines. (*A*) Initial EPSCaT potency ($P = 0.57$) and initial spine volume ($P = 0.93$) was not different for spines that persisted for 7 d ($n = 16$ spines in 16 slice cultures) or were eliminated ($n = 5$ of 5). Two control conditions in which no LTD was induced [no oLFS, oLFS plus D-2-amino-5-phosphonopentanoic acid (APV)] were pooled for statistical analysis, as spontaneous spine elimination was a rare event. (*B*) Under conditions in which no LTD was induced, initial p_{Ca} was not different in persistent and eliminated spines ($P = 0.98$, same spines as in *A*). Black symbols indicate control spines without oLFS. Green symbols indicate control spines with APV present during oLFS. Black horizontal lines indicate mean ± SEM (*B*, *Left*, and *C*, Mann–Whitney test, two-sided; *A*, *Right*, unpaired *t* test, two-sided).